The Caspase-3 homolog DrICE regulates endocytic trafficking during *Drosophila* tracheal morphogenesis

Saoirse S. McSharry[1] and Greg J. Beitel[1*]

Key words: caspase; non-apoptotic; endocytic trafficking; morphogenesis; epithelial tube; *Drosophila*; trachea

[1]Department of Molecular Biosciences, Northwestern University, Evanston, IL 60208, USA

Running title: Caspase-mediated regulation of endocytic trafficking

* Author for correspondence and lead contact: Greg J. Beitel, Hogan Hall, Rm. 2-100, Northwestern University, Evanston, IL 60208, U.S.A., beitel@northwestern.edu, Ph: (847) 467-7776, FAX: (847) 467-1380

ABSTRACT

Although well known for its role in apoptosis, the executioner caspase DrICE has a non-apoptotic function that is required for elongation of the epithelial tubes of the *Drosophila* tracheal system. Here, we show that DrICE acts downstream of the Hippo Network to regulate endocytic trafficking of at least seven cell polarity, cell junction and apical extracellular matrix proteins involved in tracheal tube size control. We further show that tracheal cells are competent to undergo apoptosis, even though developmentally-regulated DrICE function rarely kills tracheal cells. Our results reveal a novel developmental role for caspases, a previously unidentified pool of DrICE that colocalizes with endocytic markers, and a mechanism by which the Hippo Network controls endocytic trafficking. Given published reports of *in vitro* regulation of endocytosis by mammalian caspases during apoptosis, we propose that caspase-mediated regulation of endocytic trafficking is an evolutionarily conserved function of caspases that can be deployed during morphogenesis.

Epithelial tubes of precise sizes are essential for gas exchange and nutrient delivery in animal tissues. Failure of correct tube sizing can lead to fatal disease[1, 2], yet the cellular and molecular mechanisms that regulate tube size remain poorly understood. To uncover these mechanisms, we study the tracheal system of the *Drosophila* embryo, a ramifying tubular network that serves as the fly's combined pulmonary and vascular systems[3].

The diameter of the largest tube in the tracheal system, the dorsal trunk (DT), increases two-fold as length increases ~15% over a 2.5 h period during mid-embryogenesis, and it does so with no accompanying changes in cell number[4]; DT dimensions are regulated by a complex set of interacting pathways that all rely on the endocytic system. An apical/lumenal extracellular matrix (aECM) that restricts elongation depends on regulated secretion and endocytosis of matrix-modifying proteins such as Serpentine (Serp)[5]. Basolateral cell-junctional complexes called Septate Junctions (SJs) also restrict DT dimensions. SJs contain a diverse range of proteins including the claudin-family member Kune-Kune (Kune) and the FERM-domain protein Yurt (Yrt)[6, 7]. As with the aECM, formation and maintenance of SJs require endocytic trafficking[8]. Apically-localized regulators of DT dimensions also interact with the endocytic pathway, including the polarity protein Crumbs (Crb), the transmembrane protein Uninflatable (Uif), atypical Protein Kinase C (aPKC), and the non-receptor tyrosine kinase Src42A[3, 9-11] The endocytic system therefore plays a central role in regulating diverse tracheal size determinants, but how the endocytic pathway is itself regulated in this context is poorly understood.

One candidate pathway that could regulate intracellular trafficking is the highly conserved Hippo Network (HN), which controls growth in diverse organisms and tissues[12]. Organ growth is promoted upon nuclear translocation of the HN effector Yorkie (Yki) in *Drosophila*, or its mammalian homolog Yes-Associated Protein (YAP). Yki and YAP are transcription factors that

activate genes required for growth and resistance to apoptosis, including the Inhibitors of Apoptosis (IAPs), which inactivate caspases[13]. When Yki/YAP activity is low, organ size is typically reduced due to apoptosis resulting from derepressed caspase activity[14]. However, we previously observed that loss of Yki or *Drosophila* Inhibitor of Apoptosis (DIAP1*)* causes overelongated trachea despite a normal number of cells. Thus, Yki and DIAP1 regulate tube size independently of apoptosis[15].

Here, we show that the caspase-3 homolog DrICE acts downstream of Yki and DIAP1 to regulate tracheal elongation. Instead of causing cell death, DrICE regulates endocytic trafficking of tracheal size determinants. This work reveals a novel intersection of the HN, caspases and the endocytic system that has critical functions during normal development. Consistent with previous evidence that mammalian caspases can control endocytic trafficking during apoptosis[16], we propose a model in which regulation of endocytic trafficking is an evolutionarily conserved function of caspases that can be activated with or without triggering cell death, to contribute to morphogenesis or apoptosis, depending on cellular context.

RESULTS

DrICE is necessary and sufficient for tracheal elongation downstream of the Hippo Network

We previously showed that DrICE is required for tracheal dorsal trunk elongation, potentially downstream of the HN [15]. Tracheae fail to elongate in embryos homozygous for the *DrICE$^{\Delta 1}$* allele, which deletes the DrICE coding sequence[17], but embryos mutant for Yki and DIAP1, both of which negatively regulate DrICE, have overly elongated tracheae at stage 16. These results were consistent with, but did not show, that DrICE acts downstream of Yki and DIAP1 in tracheal elongation.

We tested whether reduction of DrICE could suppress the long tracheal phenotypes caused by mutations in Yki, or its transcriptional target DIAP1, which is encoded by the *thread (th)* locus[15, 18]. Single loss-of-function mutants *yki*^{B5} and *th*^{J5C8} mutants each have elongated trachea that follow irregular sinusoidal paths (Fig. 1b,f,m), but double mutant trachea of the genotypes *yki*^{B5}; *DrICE*^{17} or *th*^{J5C8}, *DrICE*^{17} are straight and have either WT lengths or have reduced lengths of *DrICE*^{17}mutants (Fig. 1d,e,m). These results indicate that DrICE acts downstream of, or in parallel to, Yki, DIAP1 and the HN.

For the above experiments, and most of the subsequent experiments in this report, we used the *DrICE*^{17} allele, which has a point mutation[19] in a region near the substrate binding site of DrICE. However, in contrast to a previous report that *DrICE*^{17} is a protein-null allele[19], using different antibodies we find that *DrICE*^{17} generates a stable protein (Fig. 1n-o and Fig. 2e-f'''), and causes a stronger tracheal phenotype than *DrICE*$^{\Delta 1}$, the null allele[15]. Thus, *DrICE*^{17} behaves as a dominant negative allele that competes with maternally contributed DrICE (Fig. 1n-o).

To distinguish between DrICE acting "downstream of" and "in parallel to" the HN in tracheal development, we used Western blotting on stage 16 embryos to show that wild-type (WT) DrICE protein levels are elevated by approximately 50% in both *yki*^{B5} and *th*^{J5C8} mutant embryos (Fig. 1n-o). Together, these results confirm that DrICE is necessary for dorsal trunk elongation and that DrICE acts downstream of the HN.

We then asked if DrICE expression is sufficient to drive tracheal elongation without increased upstream HN activity by expressing UAS-DrICE in the tracheal system using the *breathless (btl)-Gal4* driver[20, 21]. This overexpression results in elongated tracheae without obvious cell death, similar to *yki*^{B5} and *th*^{J5C8} mutants (Fig. 1c,m and 2i-j'''). DrICE is therefore necessary and sufficient to drive tracheal elongation.

Tracheal cells are not refractory to apoptosis

Although the executioner caspase DrICE is necessary for tracheal elongation, few (<3%) tracheal cells undergo apoptosis during wild-type morphogenesis.[22] This raises the question of how a caspase can act in a developmental process without triggering apoptosis. We investigated the possibility that apoptosis maybe disabled in the developing trachea by analyzing loss-of-function mutants for the caspase inhibitor DIAP1 (th^{J5C8}). We previously showed that th^{J5C8} mutant embryos with contiguous dorsal trunks have elongated trachea despite a WT number of cells[15], but a more comprehensive analysis of th^{J5C8} mutants here revealed that the majority of th^{J5C8} embryos, are in fact missing dorsal trunk segments (Fig. 1i). Strikingly, 25% of heterozygous th^{J5C8} embryos displayed missing tracheal segments (Fig. 1l), suggesting that tracheal cells are capable of undergoing caspase-mediated apoptosis.

To directly test the apoptotic potential of tracheal cells, we expressed the pro-apoptotic genes Grim and Reaper [23] in the developing trachea using the *btl*:*Gal4* tracheal driver. Overexpression of Grim largely eliminates the tracheal system (Fig. 1g). Reaper overexpression results in the loss of one or two tracheal dorsal trunk segments in most embryos, similar to the homozygous th^{J5C8} mutant phenotype (Fig. 1h,i). Critically, the lethal effects of Grim overexpression are dominantly suppressed by one copy of the $DrICE^{17}$ allele (Fig. 1j), and homozygous $DrICE^{17}$ blocks the ability of Grim to destroy the tracheal system (Fig. 1k). Taken together, these results demonstrate that tracheal cells are not refractory to apoptosis— they have a functional caspase-dependent apoptotic system that does not kill cells during normal development, despite the requirement for DrICE in tracheal elongation.

A pool of DrICE localizes to punctae enriched at the tracheal apical surface

To explore the mechanism by which DrICE mediates tracheal elongation, we tested whether DrICE might be spatially compartmentalized in non-apoptotic cells. Staining with the α–DrICE^{SK31} antibody, raised against full-length DrICE protein[24, 25], produces a diffuse cytoplasmic signal in WT trachea that is greatly reduced in or absent from the nucleus (Fig. 2a). Notably, DIAP1, which causes DrICE degradation[24], is largely nuclear (Fig. 2o). This reciprocal localization of DrICE and DIAP1 may permit apoptotic-independent functions of DrICE in the cytosol of tracheal cells while protecting vital nuclear contents from caspase cleavage.

A different pattern of staining is observed with the α–DrICE^{CST9478} antibody, which is raised against a peptide N-terminal to the Asp230 cleavage site of DrICE and is reported to preferentially recognize the cleaved form of DrICE (Cell Signaling Technologies, #9478). α–DrICE^{CST9478} signal is localized to numerous cytosolic punctae that are enriched at the apical surface of tracheal cells (Fig. 2b',k',l',m',n',o'). Thus, there is a pool of DrICE that is localized away from the inhibitor DIAP1 and away from another general cytosolic pool of DrICE; this compartmentalization may allow DrICE to elongate the trachea without triggering apoptosis.

DrICE is associated with endocytic compartments

The punctate pattern of α–DrICE^{CST9478} signal resembles that of intracellular trafficking machinery, suggesting that this pool of DrICE may associate with trafficking compartments. We tested for colocalization of α–DrICE^{CST9478} signal with markers of endocytic vesicle formation (Clathrin), and for early (Rab5), recycling (Rab11), or late (Rab7) endosomes. Punctate DrICE^{CST9478} signal partially overlaps with Clathrin (23% overlap, Pearson R= 0.25) and Rab5 (Fig. 2k-l"), but little co-localization with Rab-11 (Fig. 2m-m"). α–DrICE^{CST9478} signal also showed little colocalization with Rab7 (2% overlap, R=0.12, Fig. 2n-n''), which marks compartments containing cargo destined for

degradation in the lysosome, even in *VPS32*/*shrub*[4] mutants in which Rab7 is clustered in patches (Supplementary Fig. 1o') due to defects in multivesicular body sorting and vesicle formation [26]. The pool of DrICE defined by α–DrICE^{CST9478} is therefore positioned to regulate tracheal size by influencing the endocytic trafficking of proteins that determine tracheal size.

DrICE associates with and alters the intracellular trafficking and/or levels of apical tracheal size determinants

Because transmembrane determinants of tracheal tube size including Crb and Uif are known to be trafficked through endocytic compartments[27, 28], we asked if DrICE associates with compartments containing these proteins. In WT stage 16 tracheae, DrICE^{CST9478} signal partially overlaps with Uif (Fig. 2b", 12% colocalization, Pearson correlation R=0.21) and Crb (Fig. 3b'', 17% colocalization, R=0.27), but shows stronger overlap with Crb at the apical surface during tube expansion at stages 13-14 (Supplementary Fig. 1b'',e''). While there is little cytosolic overlap between Crb or Uif with α–DrICE^{CST9478} staining in WT embryos, in *VPS32*/*shrub*[4] mutants, there is some overlap between α–DrICE^{CST9478} and enlarged vesicles containing Crb or Uif (arrows, Fig. 3c" and Supplementary Fig. 1s''). An apical pool of DrICE is therefore positioned to directly regulate trafficking of apical markers.

We tested if there were functional interactions between DrICE and transmembrane apical markers by examining Crb and Uif in *DrICE*[17] mutants. In stage 14 embryos, fewer Crb-positive cytosolic punctae were visible in *DrICE*[17] mutants than in WT ($p<0.05$, Fig.3a-a' and Supplementary Fig. 2a) and over-expression of DrICE in the tracheal system increases Crb levels at stage 16 ($p<0.0005$, Supplementary Fig. 4a-c). No significant changes in Uif abundance or distribution were observed in *DrICE* mutant tracheae (Fig. 2f",h", 3d',g' and Fig. 4g), but *DrICE*[17] suppresses the increased abundance of Uif positive punctae in the tracheae of embryos mutant for the

basolateral polarity protein Yurt ($p<0.05$; Fig. 4d-g and Supplementary Fig. 2d). Moreover, *DrICE*^{17} also suppresses the increased tracheal length of the *yrt*^{65A} mutants ($p<0.005$, Fig. 4h-l).

To determine if DrICE is required for the intracellular trafficking and/or levels of apically localized, non-transmembrane size determinants, we examined the effects of *DrICE*^{17} on the localization and levels of aPKC and phosphorylated Src (pSrc)[9, 10, 29] The number and intensity of aPKC punctae are dramatically increased in *DrICE*^{17} tracheal cells, similar to the increases seen in *VPS32/shrub*^{4} mutant cells (arrows, Fig. 3d-f'). pSrc is reduced at the apical membrane in both *DrICE*^{17} and *shrb*^{4} mutant trachea (Fig. 3g-i'). Together, these results demonstrate that DrICE is required for normal endocytic trafficking of diverse apical membrane size determinants.

DrICE colocalizes with and alters the trafficking of lumenal tracheal determinant Serpentine

We investigated whether DrICE is required for trafficking of lumenal determinants required for tracheal size control, including the putative chitin deacetylase Serpentine (Serp). As with the apical determinant Uif, we found that *DrICE*^{17} suppresses the overabundance of Serp-containing punctae in *yrt*^{65A} ($p<0.05$; Fig. 4f' quantified in Supplementary Fig. 2b). Furthermore, overactivation of DrICE resulting from loss of *yki* decreases the amount of lumenal Serp in tracheal anterior, a phenotype that is partially suppressed by *DrICE*^{17} ($p<0.0005$; green in Fig. 4m-p" and Supplementary Fig. 2c). DrICE therefore affects trafficking of lumenal tracheal size determinants and mediates the effects of the HN on their trafficking.

DrICE alters the trafficking of tracheal junctional components

We tested whether DrICE mutants exhibited alterations in trafficking of basolateral junctional components, which are known to be constitutively recycled through the endocytic system through tracheal development [30, 31]. Immunostaining for the claudin Kune-Kune (Kune) and for

Melanotransferrin (MTf) revealed that junctional and overall levels of Kune are reduced in *yki*^{B5} trachea ($p<0.05$; Fig. 4r and Supplementary Fig. 2d), and in trachea overexpressing DrICE (Fig. 4b'), both conditions in which DrICE is elevated. Conversely, in *DrICE*^{17} mutants, strong ectopic staining for Kune and MTf is apparent at the apical (lumenal) surface and overall levels of Kune are increased (Fig. 4s,v and Supplementary Fig. 2d). Unexpectedly, however, SJ components were not always negatively regulated by *DrICE*. For example, in *DrICE*^{17} mutants, overall levels of MTf are reduced, while those of Kune are increased (Supplementary Fig. 2d). Moreover, levels of Discs Large (Dlg), a conserved basolateral polarity protein, were increased in *yki*^{B5} mutant trachea, whereas Kune and Mtf levels were decreased (Fig. 4r, u and Supplementary Fig. 2d, f'). Together, these results reveal that DrICE activity can modulate the trafficking of cargo at both the apical and basolateral membranes, and at minimum affects the trafficking of at least seven different proteins required for tracheal size control.

DrICE is required for trafficking in non-tracheal epithelia

Is the endocytic function of DrICE a specialized function that only operates in the trachea? Immunostaining for α–DrICE^{CST9478} reveals a similar punctate pattern and overlap with Clathrin and other Rabs in the epidermis and hindgut, as in the trachea (Supplementary Fig. 1n and Supplementary Fig. 3a-e"). Moreover, in the epidermis and hindgut, *DrICE*^{17} alters trafficking of apical, lumenal and junctional proteins, including Crb, aPKC, pSrc, Kune, MTf, and Dlg, although not always in the same way as in the trachea (Fig. 3j-r" and Supplementary Fig. 4a-i", 4j'-o' and Supplementary Fig. 2e'-g'). For instance, levels of MTf decrease in *yki*^{B5} trachea and epidermis (Fig. 4n-n'), but they appear to increase in *yki*^{B5} hindgut (Fig. 5h'). Critically, the excess of apical Serp in *yrt* mutant hindgut and epidermis is also suppressed by *DrICE*^{17} (Fig. 5a-f'). DrICE is therefore required for the correct trafficking of apical, secreted, and junctional proteins in multiple developing epithelial tissues.

DISCUSSION

Our work shows for the first time that a caspase regulates endocytic trafficking during normal morphogenesis. Moreover, the caspase activity responsible for the endocytic function does not trigger apoptosis, even though the cells are competent to undergo caspase-mediated apoptosis. We also demonstrate a previously unidentified link between the Hippo Network (HN) and the endocytic system. While previous studies focused on the effects of the endocytic system on the *output* of the Hippo Network[32-35], we report the converse: the Hippo Network acts as *input* to the endocytic system that alters endocytic trafficking.

The mechanism by which tracheal cells avoid death in the face of activated caspases may involve spatial compartmentalization of multiple components of apoptotic machinery. First, a pool of DrICE localizes to the endocytic system, which may help limit DrICE function to the endocytic pathway. Second, the caspase inhibitor DIAP1 is predominantly localized to the nucleus—this reciprocal localization of the caspase and its inhibitor may serve two purposes: (i) nuclear localization of DIAP1 may help the cell survive by limiting caspase cleavage of vital nuclear substrates, and (ii) nuclear localization of DIAP1 may make the cytosol a more permissive environment for non-apoptotic caspase function. The nuclear localization of DIAP1 in tracheal and hindgut cells is in marked contrast to the cytosolic localization of DIAP1 in salivary glands (Shukla and Tapa 2011) and the ventral nerve cord[36], indicating that as yet unidentified mechanisms regulate DIAP1 localization.

The counterintuitive requirement of an executioner caspase to promote growth in an epithelium has not previously been reported in mammals. However, there is *in vitro* evidence that mammalian caspases regulate endocytic trafficking[16]. For example, Duclos et al. showed that activation of activator and effector caspases in HeLa and HEK293 cells resulted in cleavage of Sorting Nexins

1 and 2 (SNX1 and SNX2), which control intracellular trafficking of specific cargos[37]. Caspase cleavage of SNX resulted in altered activation of the hepatocyte growth factor receptor (HGFR) and ERK1/2 signaling. Additionally, Han et al. showed that caspase-3 cleavage of junctional component Gap43 was required for endocytosis of the AMPA receptor A in non-apoptotic cells in vitro[38]. Together, the previously published *in vitro* mammalian results and these *in vivo Drosophila* results suggest a new developmental role for caspase-mediated regulation of endocytic trafficking that is evolutionarily conserved and may also function in mammalian development.

The conserved involvement of caspases in endocytic trafficking raises the possibility that there is a deeper mechanistic connection between apoptosis and trafficking of junctional components. In the current model of apoptosis, caspase-mediated proteolysis of cell junctions results in decreased cell adhesion, which allows an apoptotic cell to be cleanly extruded from an epithelium (Fig. 4p, middle; reviewed by[39]). However, in mammals and flies, junctional components are constitutively cycled through the endocytic system even in non-apoptotic epithelia[30, 31, 40]. This presents an opportunity for caspases to alter trafficking of junctional components. Perhaps the ability of caspases to regulate endocytic trafficking arose as an ancient apoptotic function that allowed dying epithelial cells to more efficiently downregulate junctions by using both endocytosis and caspase-mediated proteolysis rather than caspase-mediated proteolysis alone. In this model, caspase-mediated rerouting of endocytosed junctional components to the lysosome allows apoptotic cells to more rapidly and robustly downregulate cell junctions to facilitate epithelial extrusion (Fig. 4p, bottom). We hypothesize that caspase-mediated alterations in cell junction trafficking has been co-opted in morphogenesis, when growing epithelia require rapid remodeling of junctional components (Fig. 4p, top).

Experimental evidence from mammalian cerebral ischemic injury supports the proposed model that limited activation of caspases alters junctional endocytosis. During cerebral ischemic injury,

blood flow in the brain is blocked, which leads to extensive caspase activation, downregulation of claudin-based tight junctions, and a large and damaging increase in vascular permeability[41]. Pretreatment of tissue with caspase inhibitors increases junctional continuity and integrity including junction components claudin-5 and the tight junction marker ZO-1, and ultimately reduces tissue damage. Strikingly, more endothelial cells show caspase activation than undergo apoptosis, suggesting that caspase activation is sufficient to induce junctional downregulation and vascular permeability.

The ability of caspases to regulate endocytic trafficking has significant implications for cancer treatments, which frequently result in caspase activation. Sub-apoptotic activation of effector caspases in surviving tumor cells after anti-cancer treatment could potentially result in reduced junctional integrity, which could further promote epithelial-to-mesenchymal transformation (EMT) and metastasis. Additionally, caspase-driven changes in the trafficking of polarity proteins, such as Crb and aPKC, and of growth factor receptors could also contribute to EMT and disease progression. Consistent with this possibility, previous evidence has indicated that caspase-3 is required for tumor cell repopulation upon irradiation[42].

In summary, this work reveals a novel function of the effector caspase DrICE during development: modulating endocytic trafficking of cell junctional components and signaling molecules. Given that mammalian effector caspases can also modulate endocytic trafficking, we propose that regulation of the trafficking of junctional components is a conserved caspase function that can be brought into play during normal morphogenesis or in pathologic conditions by localized, sub-apoptotic caspase activation.

FIGURE LEGENDS

Fig. 1: The executioner caspase DrICE acts downstream of the Hippo Network to elongate tracheal tubes during development without triggering apoptosis.

(a-l) Compared to WT (w^{1118}, stage 16) (a), the dorsal trunks (DTs) of yki^{B5} mutant embryos and embryos expressing full-length DrICE in the tracheal system (*btl>DrICE*) are elongated (b,c), while DTs in $drICE^{17}$ are too short (d). $DrICE^{17}$ is epistatic to yki^{B5} since yki^{B5}; $DrICE^{17}$ double mutants do not have long trachea (e). Loss of the DrICE inhibitor DIAP/*th* can cause tracheal over-elongation (f), but also causes missing DT segments when homozygous (i) or heterozygous (l). Tracheal expression of the pro-apoptotic genes *Grim* (g) or *Reaper* (h) causes severe or moderate segment loss, respectively (g, h), that is partially or fully suppressed by one or two copies of $DrICE^{17}$ (j, k). Red arrows in G mark remnants of the tracheal system, while yellow arrowheads in h-l mark missing dorsal trunk segments. Scale bar for a-l in a, 25 μm.

(m) Quantification of DT length in single and double mutant combinations of HN and DrICE mutants, and in embryos overexpressing DrICE. DT length normalized to w^{1118} for HN and DrICE mutants, and to *btl-Gal4, UAS-GFP/+* for overexpressed DrICE (*btl-Gal4 UAS-GFP/+; UAS-DrICE/+*). Error bars, S.E.M.

(n,o) Western blots of stage 16 embryos using the α-DrICE^{CST13085} antibody that recognizes full-length DrICE. yki^{B5} and th^{J5C8} mutations increase DrICE levels (n, top). Quantification of the 47kDa DrICE full-length band relative to total protein from three experiments (o). DrICE protein levels in $DrICE^{17}$ homozygotes are not different than WT, which is consistent with $DrICE^{17}$ being a dominant negative allele that causes more severe tracheal phenotypes than the DrICE$^{\Delta 1}$ null allele[15](n,o). *p<0.05; **, p<0.005; ***, p<0.0005.

Fig. 2: A pool of DrICE co-localizes with markers of the endocytic system.

(a-j"') Staining with the α-DrICE^{SK31} antibody against full-length DrICE (a,c,e,g,i) reveals broad cytoplasmic signal in WT trachea (a) that is reduced in trachea zygotically homozygous for the null allele *DrICE$^{\Delta 1}$* (g) and elevated in trachea overexpressing DrICE (i). Staining with α-DrICE^{CST9478} (b,d,f,h, j), which was raised against a peptide containing the DrICE sequence that is cleaved during activation, reveals a more restricted punctate pattern that is enriched at the tracheal apical surface in WT trachea at stage 16 (yellow arrows, b), and even more enriched at earlier developmental stages (Supplemental Fig. 1b,e). α-DrICE^{CST9478} signal is reduced in *DrICE$^{\Delta 1}$* trachea (h) and elevated in trachea overexpressing DrICE (j).

(k-n") Colocalization of DrICE^{CST9478} signal with markers of the endocytic system in WT *(w^{1118})* trachea. α-DrICE^{CST9478} signal shows partial colocalization with Clathrin (k) and Rab5 (l), but not with Rab11 (m) or Rab7 (n).

(o-o") The DrICE inhibitor DIAP1 has predominantly nuclear localization (o) that is largely the converse of the cytosolic DrICE^{CST9478} staining (o').

(p) Partial schematic of the endocytic system showing the roles of endocytic markers.

Scale bar for a-j" in j", 5 μm; Scale bar for k-o" in o", 5 μm.

Fig. 3: DrICE is required for normal levels and localization of the tracheal size determinants Crb, pSrc and aPKC in the trachea and epidermis

(a-i") The number of cytosolic Crb punctae is decreased in *DrICE^{17}* mutants at stage 14 (a', arrowheads) compared to WT (a, and Supplemental Fig. 2A). At stage 16, α-DrICE^{CST9478} signal partially overlaps with Crb at the apical surface in WT trachea (b, arrows), and Crb colocalizes with DrICE in aberrant cytosolic structures in *VPS32/shrub^{4}* trachea (c, arrows). In *DrICE^{17}* mutants, aPKC levels are increased (d), while pSrc levels are decreased, particularly at the apical surface (g, yellow lines). Uif staining marks the apical surface.

(j-r'') *DrICE*^{17} affects the levels and/or localization of Crb, aPKC and pSrc in the epidermis. Crb, aPKC, and pSrc levels are increased in *DrICE*^{17} epidermis, particularly at the apical surface (j,m,p, arrows). Crb, aPKC and pSrc levels and/or localization are also strongly affected by in the endocytic mutant *VPS32/shrub*^{4} (l,o,r).

Fig. 4: DrICE is required for endocytic trafficking of lumenal and basolateral tracheal size determinants.

(a-c) Overexpression of DrICE in the trachea decreases Kune levels relative to the control (a' vs. b'), consistent with the overabundance of Kune in *DrICE*^{17} mutants. Conversely, Crb levels are increased when DrICE is overexpressed (a vs. b). The mean intensity of Crb is quantified relative to the control (c). Stage 16 embryos. Scale bar for a-b" in b", 5 μm. ***, $p<0.0005$

(d-g') Mutation of the basolateral polarity protein Yurt (*yrt*^{65A}) causes abnormal intracellular accumulation of the tracheal size determinants Uif (e, arrow) and Serp (e', arrow), an effect that is suppressed by *DrICE*^{17} (f-f'). White dashed lines outline tracheal cytoplasm. Quantification of punctae number in Supplementary Fig. 2b. Scale bar d-g', 5 μm.

(h-l) The *DrICE*^{17} mutation suppresses tracheal overelongation caused by a mutation in the basolateral polarity gene *yrt* (h-l). Quantification of tracheal DT length at stage 16 for *yurt*^{65a} and *yurt*^{65A}, *DrICE*^{17} and *DrICE*^{17} mutants reveals that *yurt*^{65A}, *DrICE*^{17} double mutants are shorter than *yurt*^{65A} mutants (l). Tracheal lengths normalized to WT (*w*^{1118}). Trachea visualized with the 2A12/Gasp monoclonal antibody. Scale bar for h-l in H, 25 μm.

(m-p'') Mutation of the Hippo Network component Yki (*yki*^{B5}) reduces the levels of Serp (green) in the tracheal anterior relative to the lumenal chitin binding protein Gasp, marked by staining with the monoclonal antibody 2A12 (arrow, n'). This reduction is suppressed by *DrICE*^{17} (o'), particularly in the anterior (arrows). Quantification of Serp and 2A12 staining in Supplementary Fig. 2c. Scale bar m-p'' in p", 25 μm.

(q-s') Kune signal in stage 16 trachea is reduced in *yki*^{B5} mutants (r), and relocalized to the apical surface in *DrICE*^{17} mutants (s). Kune signal is also reduced in the epidermis in *yki*^{B5} mutants (r') and is more diffuse and cytoplasmic in *DrICE*^{17} mutants (s'). Dashed yellow lines outline the trachea apical surface in q-s and t-v. Quantification of Kune levels in Supplementary Fig. 2d. Scale bar for q-v' in v', 5 μm.

(t-v') MTf signal in stage 16 trachea is reduced in *yki*^{B5} mutants (u), and relocalized to the apical surface in *DrICE*^{17} mutants (v). MTf signal is also reduced in the epidermis in *yki*^{B5} mutants (u') but is not as strongly affected in *DrICE*^{17} mutants (v'). Quantification of MTf levels in Supplementary Fig. 2d. Scale bar for q-v' in v', 5 μm.

Fig. 5:

(a-f') In the hindgut (a-c') and in the epidermis (d-f'), a mutation in the basolateral polarity gene *yrt* increases levels of the apical size determinant UIF and the lumenal size determinant Serp (b, b', e and e'). In both tissues, this increase is suppressed by a *DrICE*^{17} mutation (c, c', f and f'). Scale bar for a-f' in f', 5 μm.

(g-i') In the hindgut, trafficking of the SJ component Kune is largely unaffected in *DrICE*^{17} and *yki*^{B5} mutants (g-i). However, trafficking of MTf in the hindgut is affected (g'-i') with MTf accumulating in *yki*^{B5} mutants (h', arrow) and showing little junctional localization in *DrICE*^{17} (i', arrow). Scale bar for g-i' in i', 5 μm.

Fig. 6 Model for caspase-regulated endocytic trafficking in apoptosis

See main text for details.

ACKNOWLEDGEMENTS

For reagents we thank Rob Ward (α-Uif), Pascal Meier (α- DrICE^{SK31}), Christos Samakovlis (α-MTf), Matthias Behr (α-Clathrin). We also thank Benjamin Kraft for assistance in epistasis experiments; Andreas Bergmann for helpful discussions; J. Hornick and the Northwestern University Biological Imaging Facility for technical and imaging support; and Laura Lackner, Heike Fölsch, and I. Tanelli Helenius for comments on the manuscript. Stocks obtained from the Bloomington Drosophila Stock Center (NIH P40OD018537) were used in this study, and FlyBase was a critical resource [43]. This work was supported by NIH RO1GM108964 to GJB. S. McSharry was supported by the National Institute of General Medical Sciences training grant T32GM008061.

AUTHOR CONTRIBUTIONS

SM and GJB conceived and designed the experiments. SM performed the experiments. SM and GJB analyzed the data. SM and GJB wrote the manuscript.

DECLARATION OF INTERESTS

All authors declare no competing interests.

REFERENCES

1. Cooper, A.D., Campeau, N.G. & Meissner, I. Susceptibility-weighted imaging in familial cerebral cavernous malformations. *Neurology* **71**, 382 (2008).
2. Faguer, S. *et al.* Massively enlarged polycystic kidneys in monozygotic twins with TCF2/HNF-1beta (hepatocyte nuclear factor-1beta) heterozygous whole-gene deletion. *American journal of kidney diseases : the official journal of the National Kidney Foundation* **50**, 1023-1027 (2007).
3. Zuo, L., Iordanou, E., Chandran, R.R. & Jiang, L. Novel mechanisms of tube-size regulation revealed by the Drosophila trachea. *Cell Tissue Res* **354**, 343-354 (2013).
4. Beitel, G.J. & Krasnow, M.A. Genetic control of epithelial tube size in the Drosophila tracheal system. *Development* **127**, 3271-3282 (2000).
5. Tsarouhas, V. *et al.* Sequential pulses of apical epithelial secretion and endocytosis drive airway maturation in Drosophila. *Developmental cell* **13**, 214-225 (2007).

6. Nelson, K.S., Furuse, M. & Beitel, G.J. The Drosophila Claudin Kune-kune is required for septate junction organization and tracheal tube size control. *Genetics* **185**, 831-839 (2010).
7. Laprise, P. *et al.* Epithelial polarity proteins regulate Drosophila tracheal tube size in parallel to the luminal matrix pathway. *Current biology : CB* **20**, 55-61 (2010).
8. de Vreede, G. *et al.* The Scribble module regulates retromer-dependent endocytic trafficking during epithelial polarization. *Development* **141**, 2796-2802 (2014).
9. Nelson, K.S. *et al.* Drosophila Src regulates anisotropic apical surface growth to control epithelial tube size. *Nature cell biology* **14**, 518-525 (2012).
10. Forster, D. & Luschnig, S. Src42A-dependent polarized cell shape changes mediate epithelial tube elongation in Drosophila. *Nature cell biology* **14**, 526-534 (2012).
11. Zhang, L. & Ward, R.E.t. uninflatable encodes a novel ectodermal apical surface protein required for tracheal inflation in Drosophila. *Developmental biology* **336**, 201-212 (2009).
12. Yu, F.X., Zhao, B. & Guan, K.L. Hippo Pathway in Organ Size Control, Tissue Homeostasis, and Cancer. *Cell* **163**, 811-828 (2015).
13. Salvesen, G.S. & Duckett, C.S. IAP proteins: blocking the road to death's door. *Nature reviews. Molecular cell biology* **3**, 401-410 (2002).
14. Verghese, S., Bedi, S. & Kango-Singh, M. Hippo signalling controls Dronc activity to regulate organ size in Drosophila. *Cell death and differentiation* **19**, 1664-1676 (2012).
15. Robbins, R.M., Gbur, S.C. & Beitel, G.J. Non-canonical roles for Yorkie and Drosophila Inhibitor of Apoptosis 1 in epithelial tube size control. *PloS one* **9**, e101609 (2014).
16. Duclos, C., Lavoie, C. & Denault, J.B. Caspases rule the intracellular trafficking cartel. *FEBS J* **284**, 1394-1420 (2017).
17. Muro, I. *et al.* The Drosophila caspase Ice is important for many apoptotic cell deaths and for spermatid individualization, a nonapoptotic process. *Development* **133**, 3305-3315 (2006).
18. Huang, J., Wu, S., Barrera, J., Matthews, K. & Pan, D. The Hippo signaling pathway coordinately regulates cell proliferation and apoptosis by inactivating Yorkie, the Drosophila Homolog of YAP. *Cell* **122**, 421-434 (2005).
19. Xu, D. *et al.* The effector caspases drICE and dcp-1 have partially overlapping functions in the apoptotic pathway in Drosophila. *Cell death and differentiation* **13**, 1697-1706 (2006).
20. Brand, A.H. & Perrimon, N. Targeted gene expression as a means of altering cell fates and generating dominant phenotypes. *Development* **118**, 401-415 (1993).
21. Shiga, Y., TanakaMatakatsu, M. & Hayashi, S. A nuclear GFP beta-galactosidase fusion protein as a marker for morphogenesis in living Drosophila. *Dev Growth Differ* **38**, 99-106 (1996).
22. Baer, M.M. *et al.* The role of apoptosis in shaping the tracheal system in the Drosophila embryo. *Mechanisms of development* **127**, 28-35 (2010).
23. Goyal, L., McCall, K., Agapite, J., Hartwieg, E. & Steller, H. Induction of apoptosis by Drosophila reaper, hid and grim through inhibition of IAP function. *The EMBO journal* **19**, 589-597 (2000).
24. Ditzel, M. *et al.* Inactivation of effector caspases through nondegradative polyubiquitylation. *Molecular cell* **32**, 540-553 (2008).

25. Zachariou, A. *et al.* IAP-antagonists exhibit non-redundant modes of action through differential DIAP1 binding. *Embo Journal* **22**, 6642-6652 (2003).
26. Gao, F.B., Brenman, J.E., Jan, L.Y. & Jan, Y.N. Genes regulating dendritic outgrowth, branching, and routing in Drosophila. *Genes & development* **13**, 2549-2561 (1999).
27. Dong, B., Hannezo, E. & Hayashi, S. Balance between apical membrane growth and luminal matrix resistance determines epithelial tubule shape. *Cell reports* **7**, 941-950 (2014).
28. Olivares-Castineira, I. & Llimargas, M. EGFR controls Drosophila tracheal tube elongation by intracellular trafficking regulation. *PLoS genetics* **13**, e1006882 (2017).
29. Francis, D. & Ghabrial, A.S. Compensatory branching morphogenesis of stalk cells in the Drosophila trachea. *Development* **142**, 2048-2057 (2015).
30. Tiklova, K., Senti, K.A., Wang, S., Graslund, A. & Samakovlis, C. Epithelial septate junction assembly relies on melanotransferrin iron binding and endocytosis in Drosophila. *Nature cell biology* **12**, 1071-1077 (2010).
31. Peglion, F., Llense, F. & Etienne-Manneville, S. Adherens junction treadmilling during collective migration. *Nature cell biology* **16**, 639-651 (2014).
32. Kwon, Y. *et al.* The Hippo signaling pathway interactome. *Science* **342**, 737-740 (2013).
33. Wang, W. *et al.* Defining the protein-protein interaction network of the human hippo pathway. *Molecular & cellular proteomics : MCP* **13**, 119-131 (2014).
34. Couzens, A.L. *et al.* Protein interaction network of the mammalian Hippo pathway reveals mechanisms of kinase-phosphatase interactions. *Science signaling* **6**, rs15 (2013).
35. Cox, C.M. *et al.* Endosomal regulation of contact inhibition through the AMOT:YAP pathway. *Molecular biology of the cell* **26**, 2673-2684 (2015).
36. Reuveny, A., Elhanany, H. & Volk, T. Enhanced sensitivity of midline glial cells to apoptosis is achieved by HOW(L)-dependent repression of Diap1. *Mechanisms of development* **126**, 30-41 (2009).
37. Duclos, C.M. *et al.* Caspase-mediated proteolysis of the sorting nexin 2 disrupts retromer assembly and potentiates Met/hepatocyte growth factor receptor signaling. *Cell Death Discov* **3**, 16100 (2017).
38. Han, M.H. *et al.* The novel caspase-3 substrate Gap43 is involved in AMPA receptor endocytosis and long-term depression. *Molecular & cellular proteomics : MCP* **12**, 3719-3731 (2013).
39. Andrade, D. & Rosenblatt, J. Apoptotic regulation of epithelial cellular extrusion. *Apoptosis* **16**, 491-501 (2011).
40. Green, K.J., Getsios, S., Troyanovsky, S. & Godsel, L.M. Intercellular junction assembly, dynamics, and homeostasis. *Cold Spring Harbor perspectives in biology* **2**, a000125 (2010).
41. Zehendner, C.M., Librizzi, L., de Curtis, M., Kuhlmann, C.R. & Luhmann, H.J. Caspase-3 contributes to ZO-1 and Cl-5 tight-junction disruption in rapid anoxic neurovascular unit damage. *PloS one* **6**, e16760 (2011).
42. Huang, Q. *et al.* Caspase 3-mediated stimulation of tumor cell repopulation during cancer radiotherapy. *Nature medicine* **17**, 860-866 (2011).

43. Gramates, L.S. *et al.* FlyBase at 25: looking to the future. *Nucleic acids research* **45**, D663-D671 (2017).

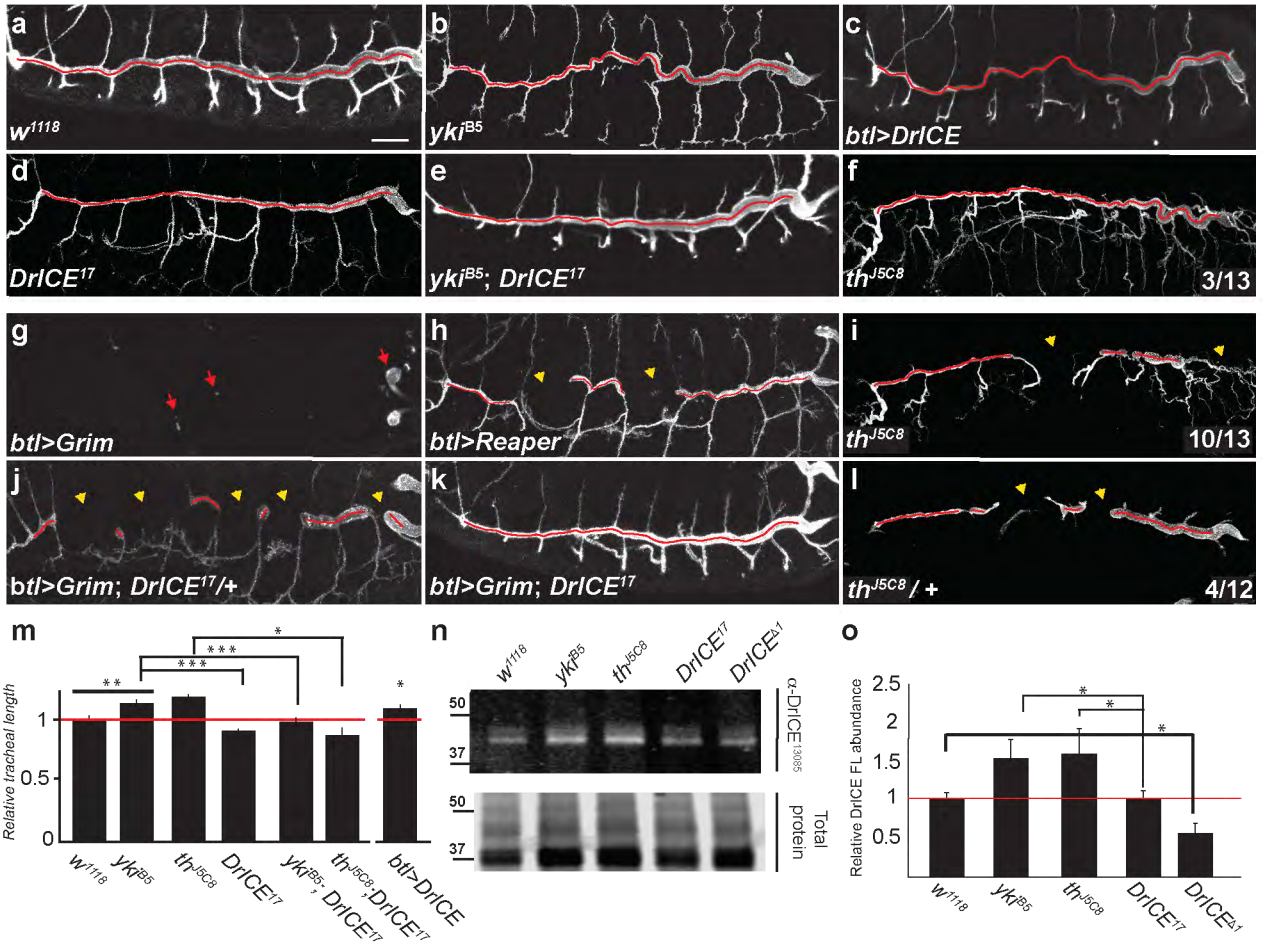
a
w1118
b
ykiB5
c
btl>DrICE
d
DrICE17
e
ykiB5; DrICE17
f
thJ5C8
3/13
g
btl>Grim
h
btl>Reaper
i
thJ5C8
10/13
j
btl>Grim; DrICE17/+
k
btl>Grim; DrICE17
l
thJ5C8 / +
4/12
m
Relative tracheal length
1
0.5
0
**
***
***
*
*
w1118
ykiB5
thJ5C8
DrICE17
ykiB5-; DrICE17
thJ5C8-;DrICE17
btl>DrICE
n
w1118
ykiB5
thJ5C8
DrICE17
DrICEΔ1
50
37
α-DrICE13085
50
37
Total protein
o
Relative DrICE FL abundance
2.5
2
1.5
1
0.5
*
*
*
w1118
ykiB5
thJ5C8
DrICE17
DrICEΔ1

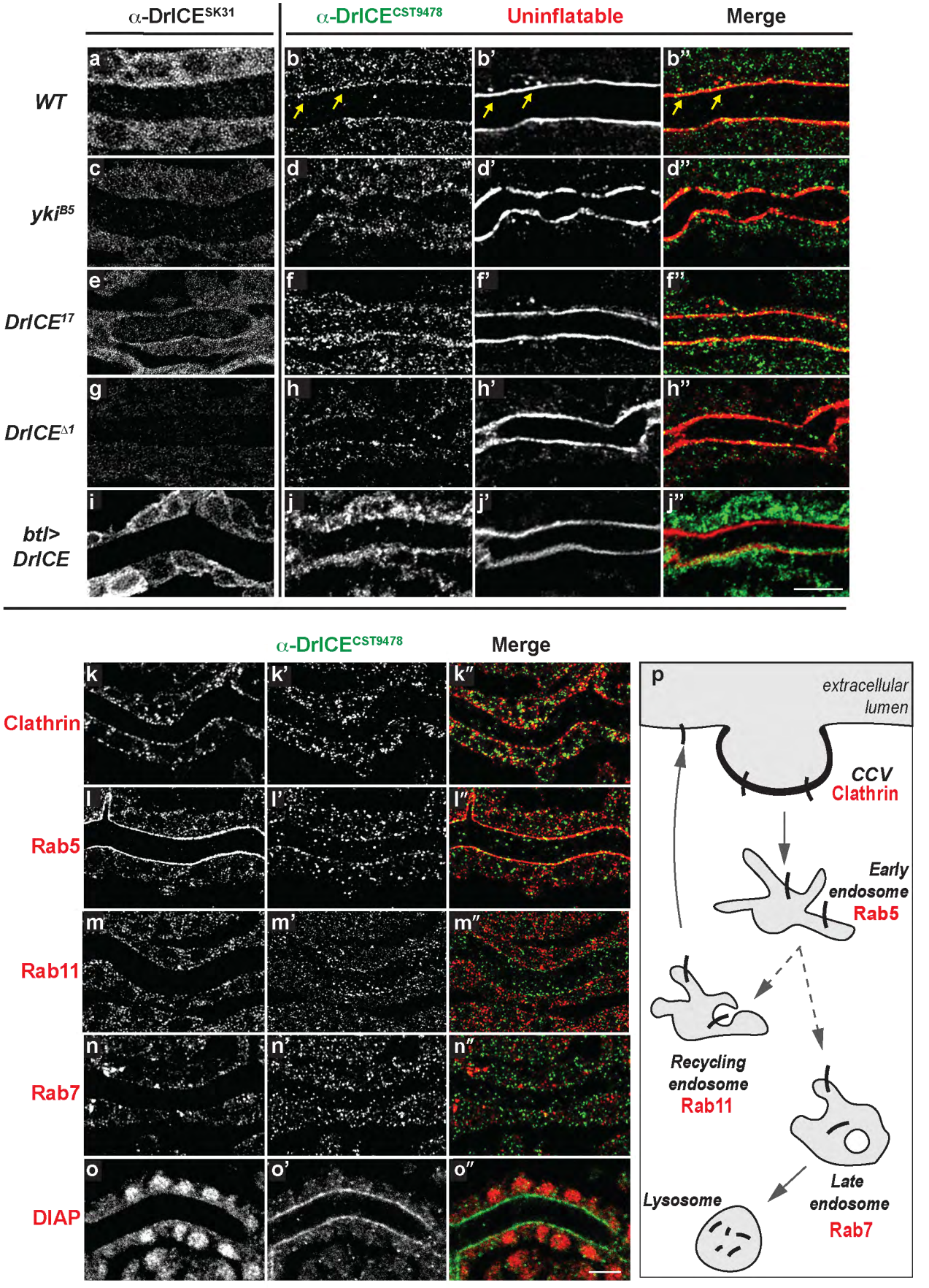
α-DrICE^SK31
α-DrICE^CST9478
Uninflatable
Merge
WT
yki^B5
DrICE^17
DrICE^Δ1
btl> DrICE
a
b
b'
b''
c
d
d'
d''
e
f
f'
f''
g
h
h'
h''
i
j
j'
j''
α-DrICE^CST9478
Merge
Clathrin
Rab5
Rab11
Rab7
DIAP
k
k'
k''
l
l'
l''
m
m'
m''
n
n'
n''
o
o'
o''
p
extracellular lumen
CCV
Clathrin
Early endosome
Rab5
Recycling endosome
Rab11
Late endosome
Rab7
Lysosome

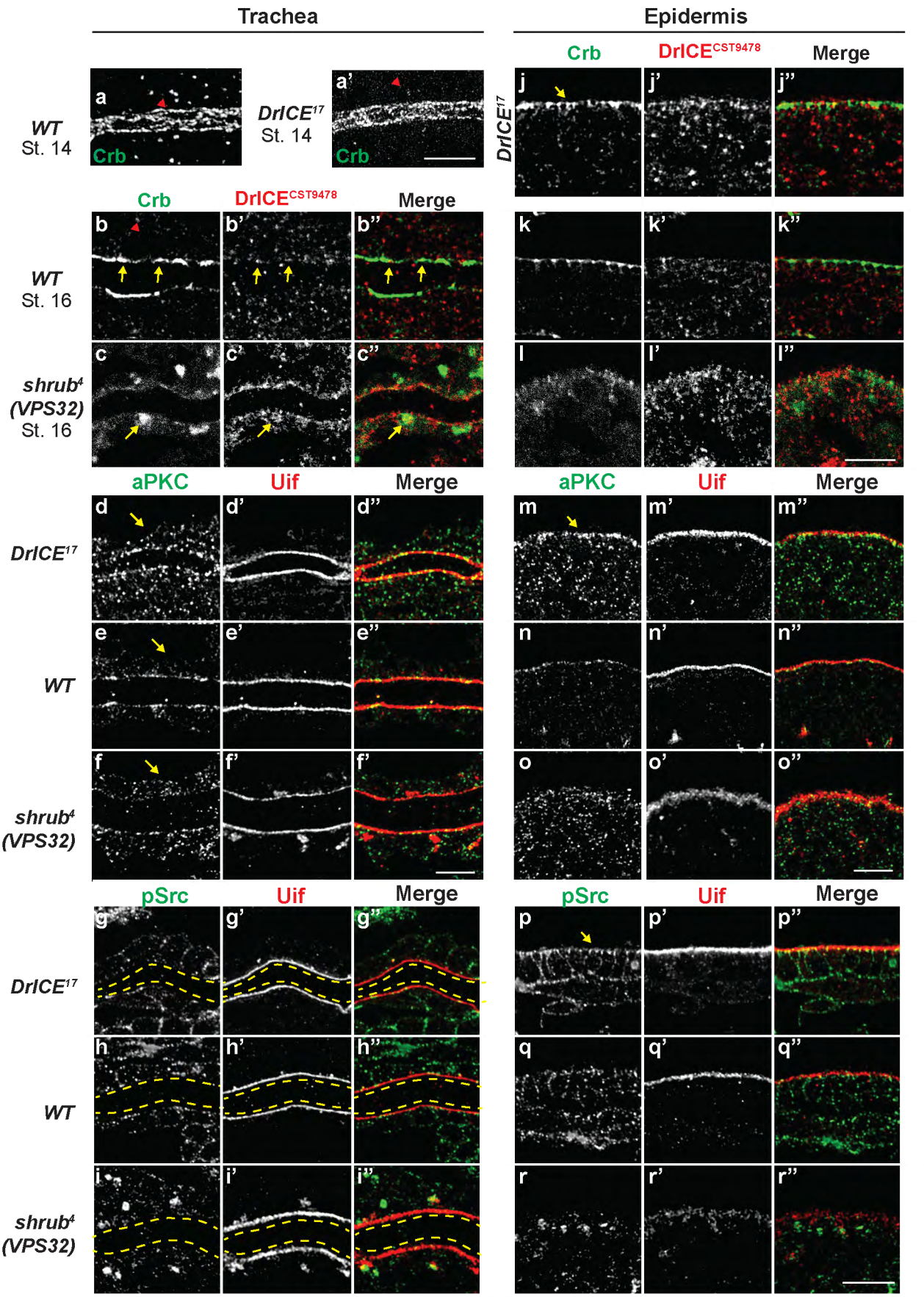
Trachea
Epidermis
WT St. 14
DrICE17 St. 14
Crb
DrICE17
Crb
DrICECST9478
Merge
WT St. 16
shrub4 (VPS32) St. 16
aPKC
Uif
Merge
DrICE17
WT
shrub4 (VPS32)
pSrc
Uif
Merge
DrICE17
WT
shrub4 (VPS32)

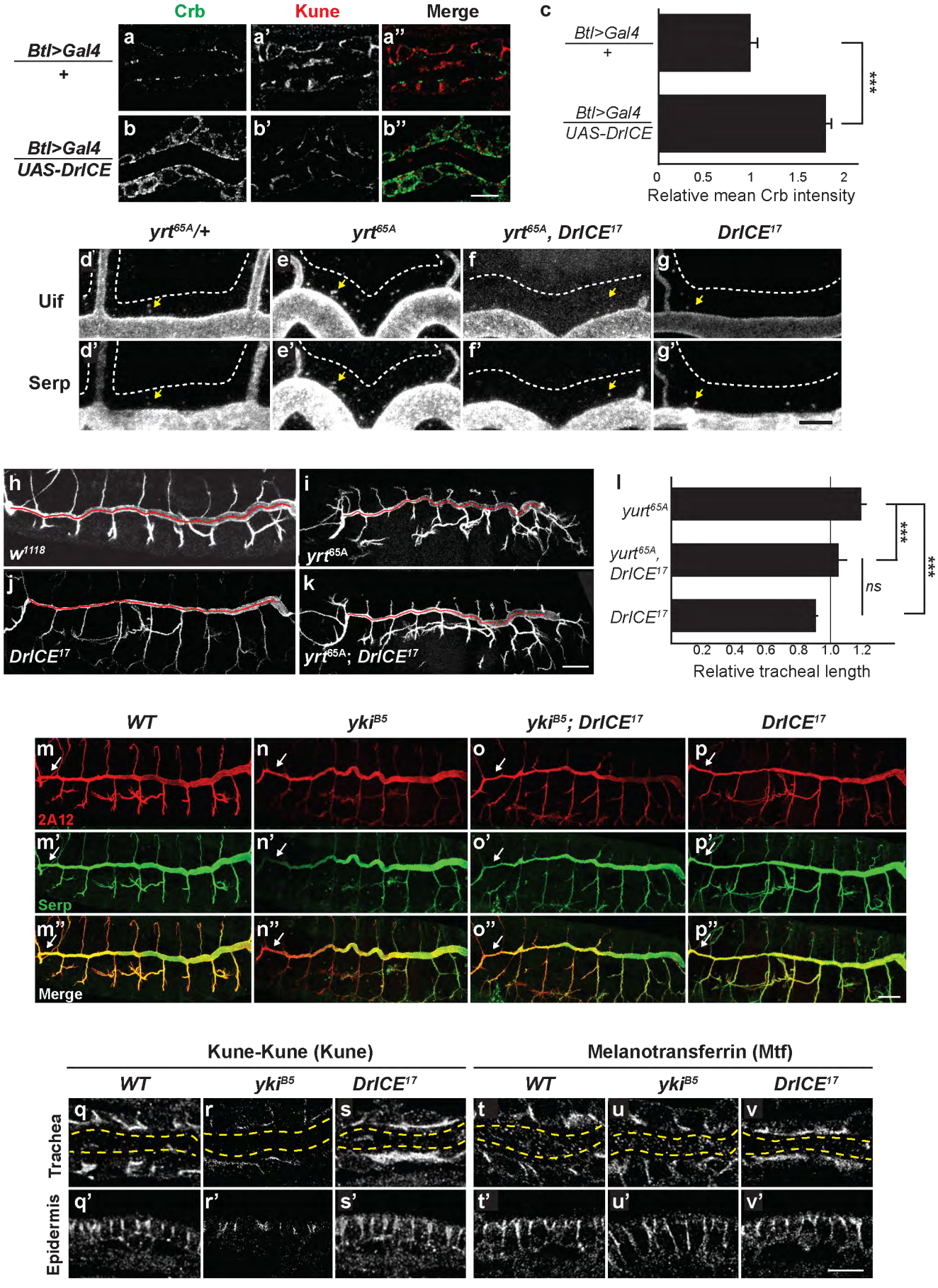
Crb
Kune
Merge
Btl>Gal4
+
Btl>Gal4
UAS-DrlCE
a
a'
a''
b
b'
b''
c
Btl>Gal4
+
Btl>Gal4
UAS-DrlCE
***
0
0.5
1
1.5
2
Relative mean Crb intensity
yrt65A/+
yrt65A
yrt65A, DrlCE17
DrlCE17
Uif
Serp
d
e
f
g
d'
e'
f'
g'
h
w1118
i
yrt65A
j
DrlCE17
k
yrt65A; DrlCE17
l
yurt65A
yurt65A, DrlCE17
DrlCE17
***
ns
***
0.2
0.4
0.6
0.8
1.0
1.2
Relative tracheal length
WT
ykiB5
ykiB5; DrlCE17
DrlCE17
m
n
o
p
2A12
m'
n'
o'
p'
Serp
m''
n''
o''
p''
Merge
Kune-Kune (Kune)
Melanotransferrin (Mtf)
WT
ykiB5
DrlCE17
WT
ykiB5
DrlCE17
Trachea
Epidermis
q
r
s
t
u
v
q'
r'
s'
t'
u'
v'

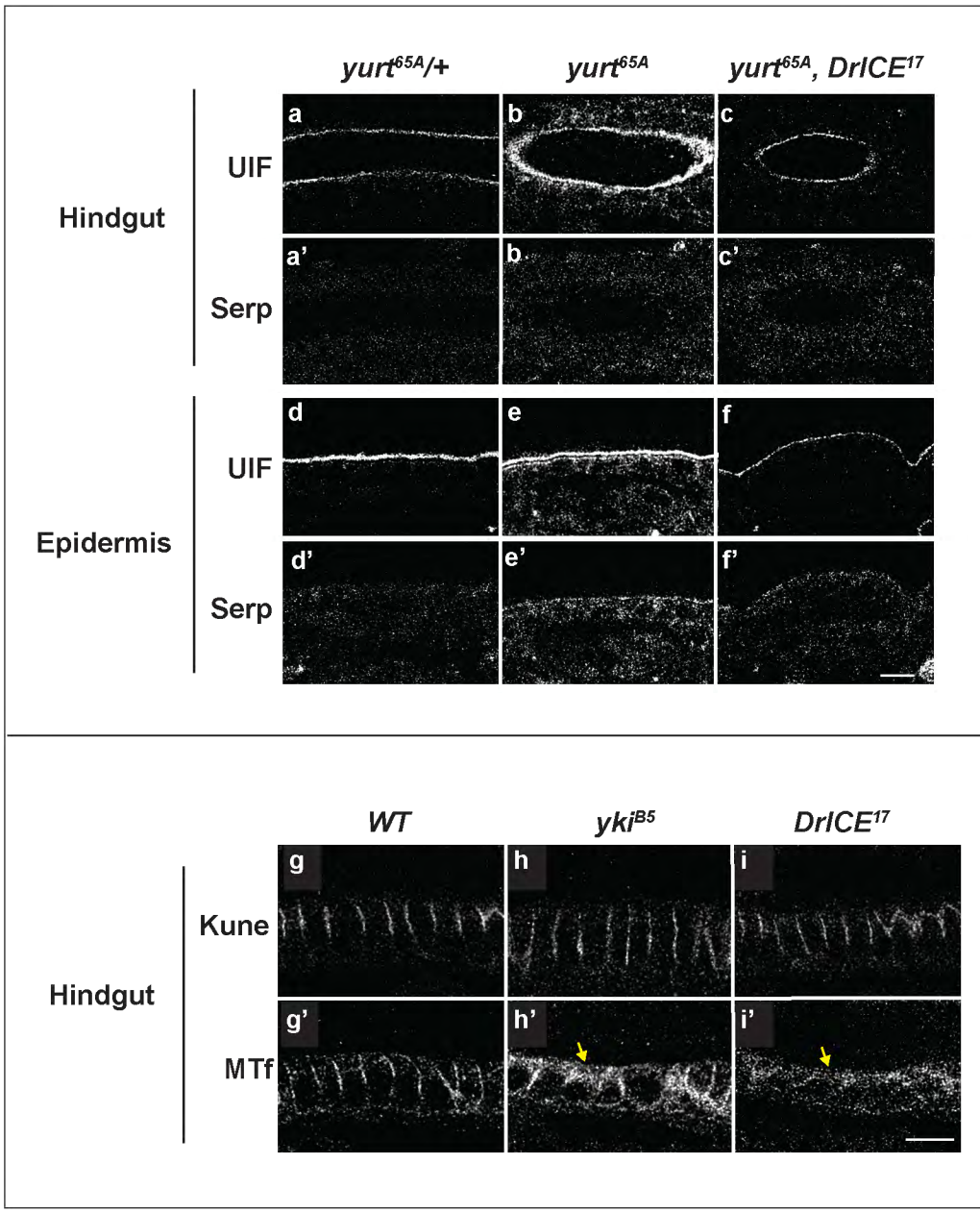
yurt65A/+
yurt65A
yurt65A, DrICE17
Hindgut
UIF
Serp
Epidermis
UIF
Serp
a
b
c
a'
b'
c'
d
e
f
d'
e'
f'
WT
ykiB5
DrICE17
Hindgut
Kune
MTf
g
h
i
g'
h'
i'

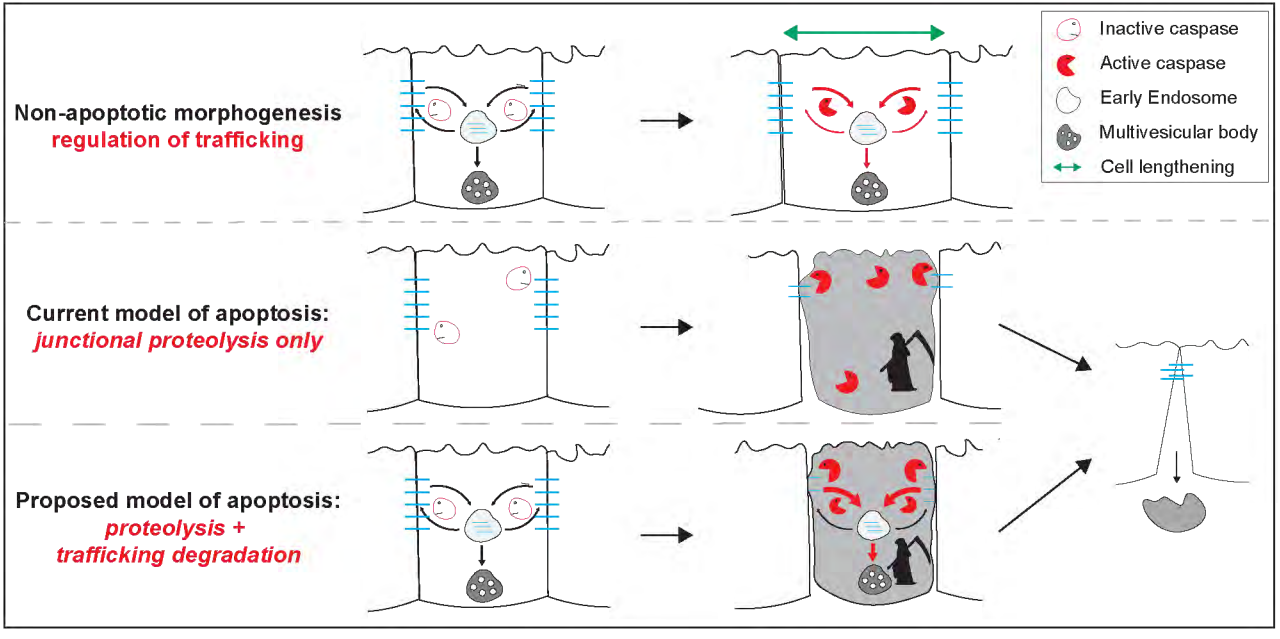
Non-apoptotic morphogenesis
regulation of trafficking
Current model of apoptosis:
junctional proteolysis only
Proposed model of apoptosis:
proteolysis +
trafficking degradation
Inactive caspase
Active caspase
Early Endosome
Multivesicular body
Cell lengthening

Supplementary Figure Legends

Supplementary Fig. 1: Developmental profile of DrICE and co-localization DrICE with markers.

(a-l) The α-DrICE^{SK31}antibody against full-length DrICE (a,d,g,j) reveals broad cytoplasmic staining at stages 13-16. Staining with α-DrICE^{CST9478} reveals a more restricted punctate pattern that is enriched at the tracheal apical surface (b,e,h,k). The apical pool of DrICE recognized by α-DrICE^{CST9478} in the trachea overlaps with staining for the apical marker Crumbs (Crb) extensively at stages 13 and 14, when endocytic trafficking of multiple tracheal size determinants drives expansion and elongation of the DT (b''-e''). In the epidermis (c,f,i,l), DrICE^{CST9478} staining shows a punctate cytosolic localization that is not enriched at the apical cell surface (arrows). Scale bar for a-l''' in L, 5 μm.

(m-p) Little colocalization of Rab7 and α-DrICE^{CST9478} is observed in WT (*shrub^{4}/+)* trachea or epidermis, even in *shrub^{4}* (*VPS32*) mutant cells where Rab7 is clustered into patches (o-o'', arrows; p). Stage 16 embryos; scale bar for m-p in p, 5 μm.

(q-t) There is some overlap between Uif and α-DrICE^{CST9478} at the apical surface in WT trachea (q-q'', arrows) and epidermis (r). In *shrub^{4}* (*VPS32*) mutant trachea, there is occasional overlap between α-DrICE^{CST9478} and enlarged ectopically accumulated vesicles containing Uif (s-s'', arrows), but essentially no overlap in the cytosol of *shrub^{4}* mutant epidermis. Stage 16 embryos; scale bar for q-t in t, 5 μm.

Supplementary Fig. 2: The levels and/or localization of junctional markers is altered in DrICE and *yki* mutants, and DrICE suppresses trafficking and length defects in *yrt* mutants.

(a) Boxplot showing that the number of cytoplasmic punctae of the apical determinant Crumbs (Crb) at embryonic stage 14 is reduced in *DrICE^{17}* tracheal cells compared to WT.

(b) Quantification of the number of cytoplasmic punctae of Uif and Serp in *yurt^{65A}/+, yrt^{65A}* and *yurt^{65A}*, *DrICE^{17}* stage 16 tracheal cells. *DrICE^{17}* suppresses the increased number of Uif and Serp punctae present in *yurt^{65A}* tracheal cells. For all panels in Supplementary Fig.2, ns = not significant; *, $p<0.05$; **, $p<0.005$; ***, $p<0.0005$.

(c) The average ratio of Serp to lumenal antigen Gasp/2A12 in the anterior lumen of the *yki^{B5}* is reduced by almost 90% compared to WT (*w^{1118})*. This reduction is partially suppressed in *yki^{B5}; DrICE^{17}* double mutant embryos. Note also that the Serp/2A12 ratio is increased in *DrICE^{17}* anterior trachea.

(d) Quantification of mean intensity of MTf and Kune in the fifth metamere of *DrICE*^{17} and *yki*^{B5} trachea from Figure 4q-v demonstrates that the overall abundance of MTf is decreased in *DrICE*^{17} trachea, while total Kune levels are increased. *w*^{1118} is used as WT.
(e-g') In the trachea (e-g) and epidermis (e'-g'), the levels of the basolateral septate junction protein Dlg are increased in *yki*^{B5} mutants and, in the trachea, reduced in *DrICE*^{17} mutants. This pattern is the opposite of the shown by another septate junction protein, Kune (Figure 4r, Supplementary Fig. 2d). Yellow lines outline tracheal lumen. Scale bar for e-g' in g', 5 μm.

Supplementary Fig. 3: In the Hindgut, α-DrICE^{CST9478} staining colocalizes with early and recycling endosomal markers, but not a late endosome marker.
(a-d) α-DrICE^{CST9478} staining colocalizes with Clathrin (endocytic vesicles, a-a"), Rab5 (early endosome, b-b") and, to a lesser extent, Rab11 (recycling endosome, c-c"). α-DrICE^{CST9478} staining does not colocalize with Rab7 (late endosome, d-d"). For Supplementary Fig. S3, all embryos are stage 16.
(e-e") In the hindgut, DIAP1 localizes predominantly to the nucleus, while α-DrICE^{CST9478} staining in present in both the cytosol and nucleus. Notably, α-DrICE^{CST9478} and DIAP staining rarely co-localize. Scale bar for a-e" in E", 5 μm

Supplementary Fig. 4: In the hindgut, levels and/or localization of apical markers are altered in *DrICE*^{17} mutants, and α-DrICE^{CST9478} staining is altered in an endocytic mutant.
(a-c") The apical marker Crb is present in cytosolic punctae in *DrICE*^{17} and *shrub*^{4} (*VPS32)* mutant hindgut cells (a-a" and c-c"), but not in WT (b-b"). For Supplementary Fig. 4, all embryos are stage 16; WT, *w*^{1118}.
(d-f") The cytosolic levels of the apical marker aPKC are elevated in in *DrICE*^{17} and *shrub*^{4} (*VPS32)* mutant hindgut cells (d-d" and f-f") compared to WT (e-e"), similar to the effects seen in *DrICE*^{17} trachea.
(G-I") Phosphorylated Src (pSrc) is reduced in the cytosol of *DrICE*^{17} mutant hindgut cells (g-g") compared to WT (h-h", arrows). Levels of pSrc are also greatly reduced in *VPS32/shrub*^{4} mutant hindgut cells (i-i", arrows), also similar to the effect seen in *DrICE*^{17} trachea. Scale bar for a-i" in i", 5 μm

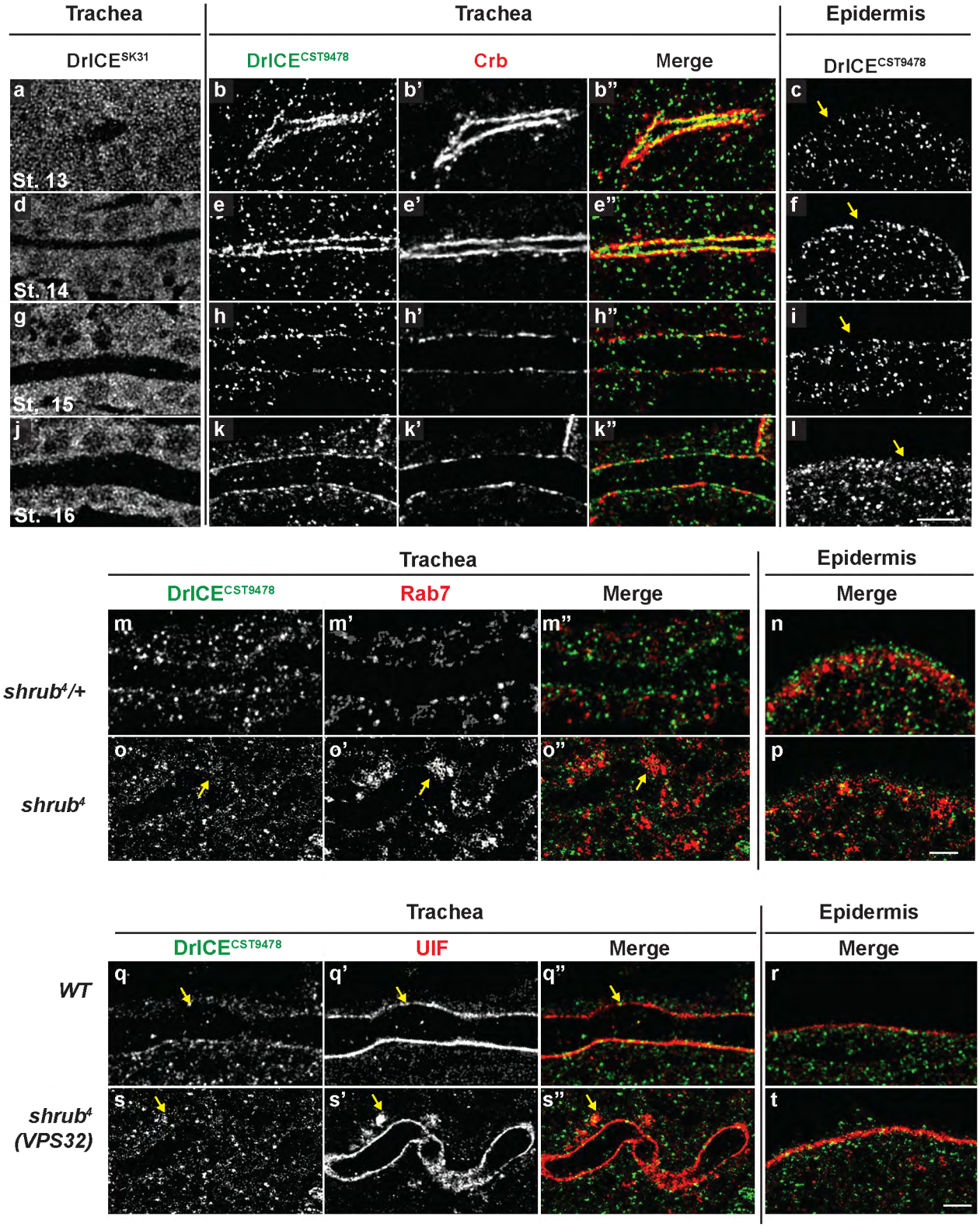
Trachea
Trachea
Epidermis
DrICE^{SK31}
DrICE^{CST9478}
Crb
Merge
DrICE^{CST9478}
a
St. 13
b
b'
b''
c
d
St. 14
e
e'
e''
f
g
St. 15
h
h'
h''
i
j
St. 16
k
k'
k''
l
Trachea
Epidermis
DrICE^{CST9478}
Rab7
Merge
Merge
shrub^4/+
shrub^4
m
m'
m''
n
o
o'
o''
p
Trachea
Epidermis
DrICE^{CST9478}
UIF
Merge
Merge
WT
shrub^4 (VPS32)
q
q'
q''
r
s
s'
s''
t

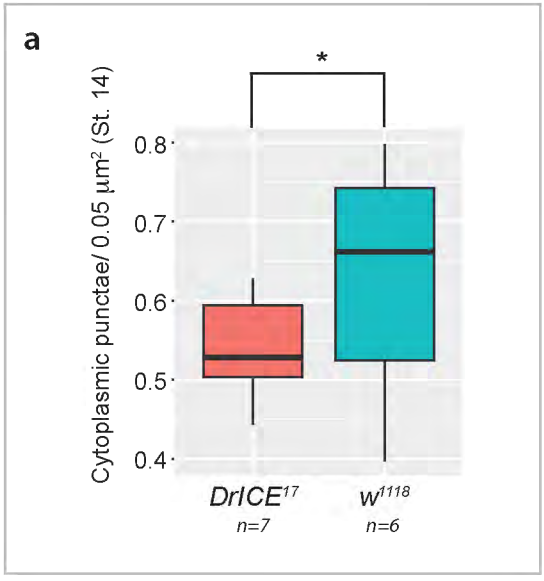
a
Cytoplasmic punctae/ 0.05 µm² (St. 14)
0.8
0.7
0.6
0.5
0.4
*
DrlCE17
n=7
w1118
n=6

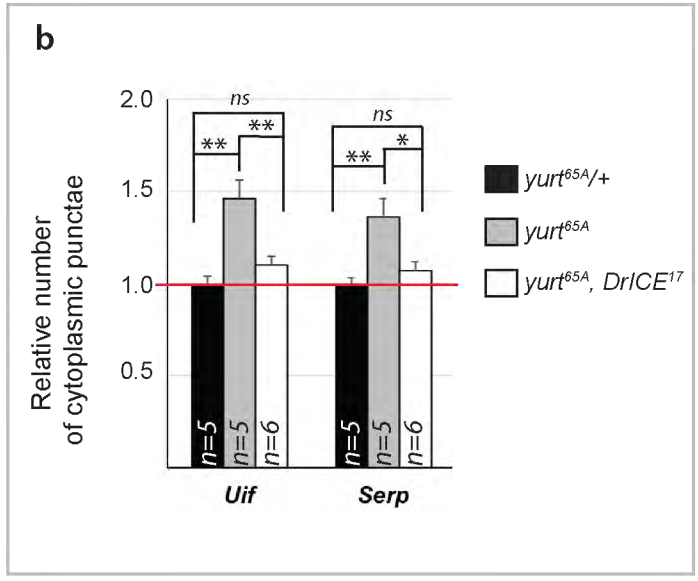
b
Relative number of cytoplasmic punctae
2.0
1.5
1.0
0.5
ns
**
**
ns
**
*
n=5
n=5
n=6
n=5
n=5
n=6
Uif
Serp
yurt65A/+
yurt65A
yurt65A, DrlCE17

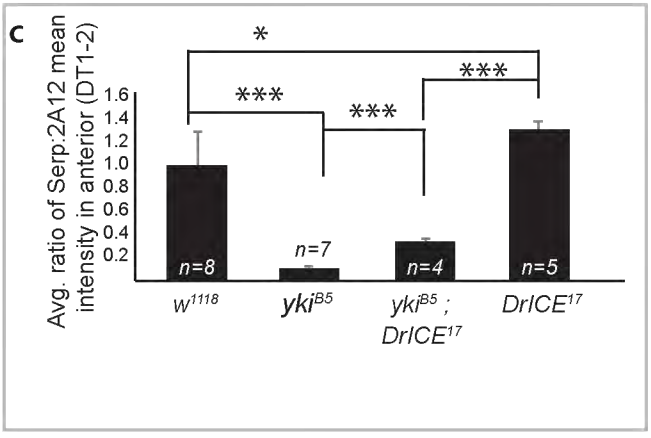
c
Avg. ratio of Serp:2A12 mean intensity in anterior (DT1-2)
1.6
1.4
1.2
1.0
0.8
0.6
0.4
0.2
*
***
***
***
n=8
n=7
n=4
n=5
w1118
ykiB5
ykiB5 ; DrlCE17
DrlCE17

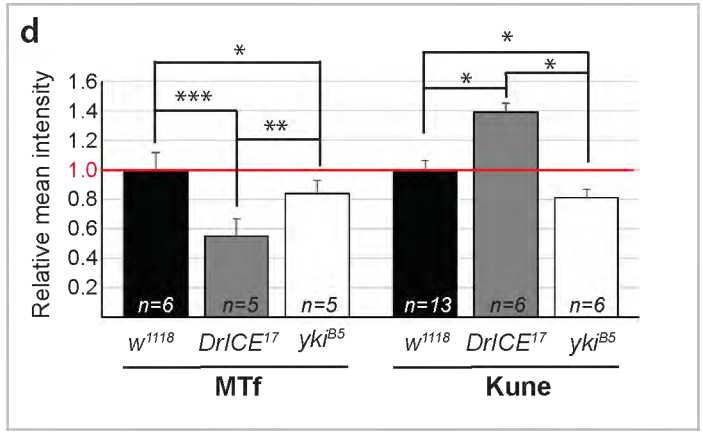
d
Relative mean intensity
1.6
1.4
1.2
1.0
0.8
0.6
0.4
0.2
*
***
**
*
*
*
n=6
n=5
n=5
n=13
n=6
n=6
w1118
DrlCE17
ykiB5
w1118
DrlCE17
ykiB5
MTf
Kune

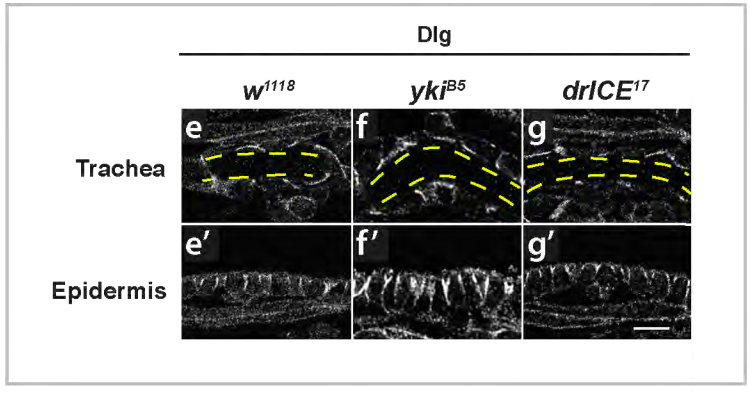
Dlg
w1118
ykiB5
drlCE17
Trachea
Epidermis
e
f
g
e'
f'
g'

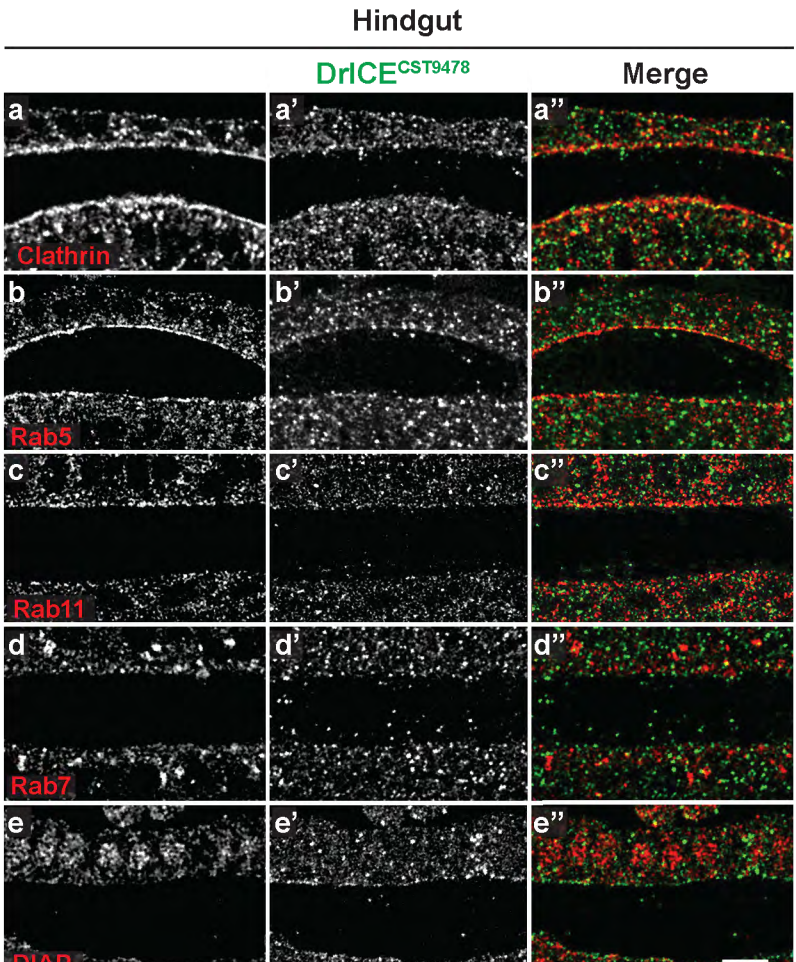
Hindgut
DrICE^{CST9478}
Merge
a
a'
a''
Clathrin
b
b'
b''
Rab5
c
c'
c''
Rab11
d
d'
d''
Rab7
e
e'
e''
DIAP

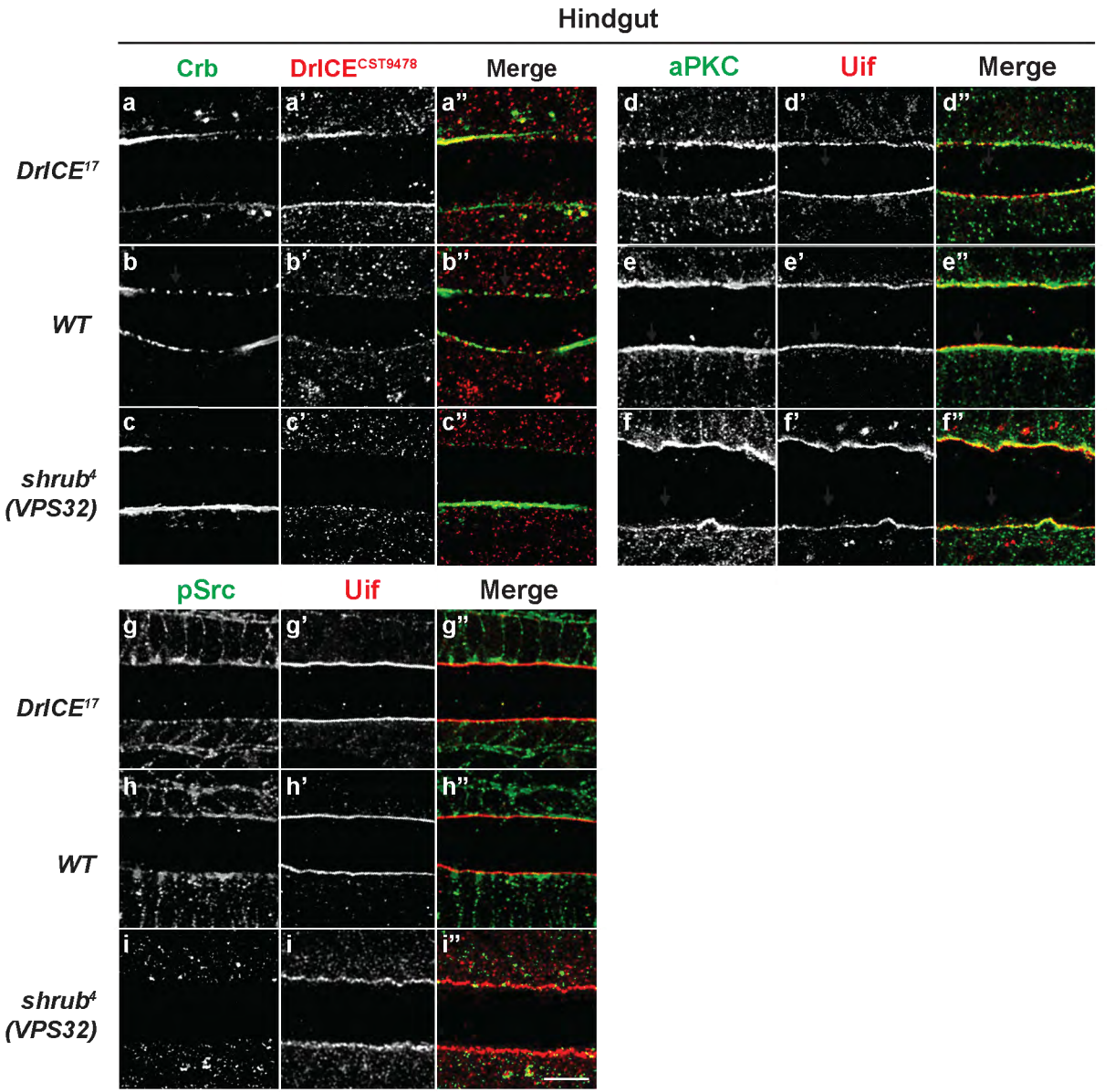
Hindgut
Crb
DrICE^{CST9478}
Merge
aPKC
Uif
Merge
DrICE^{17}
WT
shrub^{4} (VPS32)
a
a'
a''
b
b'
b''
c
c'
c''
d
d'
d''
e
e'
e''
f
f'
f''
pSrc
Uif
Merge
g
g'
g''
h
h'
h''
i
i'
i''

METHODS

Fly Stocks

The following mutant alleles were used in this paper: *th*^{J5C8} (Hay et al., 1995), *yorkie*^{B5} (Silva et al., 2006), *DrICE*^{17} (Xu et al., 2006), *DrICE*$^{\Delta 1}$ (Muro et al., 2006), *shrub*^{4} (Sweeney et al., 2006), and *yurt*^{65A} (Laprise et al., 2006). DrICE overexpression in the trachea was achieved using the UAS/Gal4 system(Brand and Perrimon, 1993). The *btl>Gal4* driver was used to express Gal4 in all tracheal cells; *btl>Gal4* flies were crossed to *UAS-DrICE* flies, which had a transgenic DrICE cDNA downstream of UAS (see *Transgenic Constructs* below). The double mutant *yurt*^{65A}*, DrICE*^{17} was generated using standard recombination crosses. Each single male resulting from the recombination crosses was screened for *yurt*^{65A} via failure to a complement *yurt*^{65A} single mutant and screened for the presence of the *DrICE*^{17} mutation by sequencing to identify the point mutation N116Y (Xu et al., 2006).

Transgenic constructs

To create the UAS-DrICE transgenic line, full length DrICE (Xu et al., 2006) cDNA sequence was cloned into the MCS of pUAST vector using Gibson cloning and subsequently inserted into the attP2 site into flies with the phiC31 integrase system.

Embryo staining

Parental flies were placed in empty food bottles capped with a molasses-agar plate spread with wet yeast. After 24 hours, plates were removed and embryos were washed with water and fixed using a protocol that largely followed that of Samakovilis et al. (2000). Embryos were dechorionated with 50% bleach for 4 minutes, and fixed in heptane with a 4% formaldehyde solution for 25 minutes. Embryos were then devitellenized for 1 minute with 100% methanol/Heptane, rehydrated to PBS-T (0.1% Triton-X100) with a methanol series, washed in PBST for 5x5' and then 3x30'. PBS-BT (3% BSA in PBS-T) was used to block for 30 minutes at RT before addition of primary antibody, in which embryos sat for 48 hours at 4 °C. See the attached chart below for appropriate dilutions. PBS-T and PBS-BT steps were repeated on the third day before addition of fluorescent secondary antibodies, in which embryos were kept O/N at 4 °C. The use of the Alexa+ secondaries (see chart for details) was essential to visualize DrICE using the α-DrICE^{CST9478} antibody as regular Alexa secondary antibodies did not have an adequate signal to noise ratio. On the final day, PBS-T washes were repeated, embryos were dehydrated using an ethanol series, and mounted with methyl salicylate and Permount mounting media (Fisher Scientific, SP15-500).

Image acquisition

Confocal z-stacks were obtained with the 63X objective on the Leica SP8 image format greater than or equal to 2048x2048, pinhole size 0.7AU, and system optimized z-step sizes of approximately 0.2 um. Images were subsequently deconvolved using Leica HyVolution software with a Huygens Essential Automatic setting. All quantification was performed on the resulting images.

Image quantification and general statistics

Quantification of junctional components was performed using ImageJ, in which a region of interest in the fifth metamere of tracheal cells was used to calculate the mean pixel intensity of each junctional component. The number of punctae for Crumbs, Uif, or Serp was calculated by acquiring the number of spots with the ImageJ SpotCounter plugin (Gaussian pre-filtering, box size=8, and noise tolerance=20) and then dividing that number by the total area of that region of interest. Each individual embryo's ratio of spots per unit area was then divided by the WT average, and a Student's 2-tailed t-test was used to calculate the p-value.

Tracheal lengths were determined by Volocity Demo 5.5.1 as previously described (Robbins et al., 2014).

Western blot

Parental flies were placed in empty food bottles capped with a molasses-agar plate spread with wet yeast. After 1 hour, plates were removed and stored in a humid chamber at 25 °C for 18 hours. Embryos were then washed with water and treated with 50% bleach for 4 minutes. The bleached embryos were sorted to collect only homozygous embryos, which lacked the fluorescent marker denoting the presence of the balancer chromosome. Approximately 30 embryos of each genotype were lysed in RIPA buffer using a micropestle, and then incubated on ice for 30 minutes before 15-minute centrifugation at 4 °C. Protein concentration of the resulting supernatant was measured by Nanodrop 2000 Spectrophotometer (ThermoFisher Scientific), and all samples were diluted with RIPA buffer to the same protein concentration before Laemmeli Buffer was added. Samples were denatured using in a boiling water bath for 5 minutes, loaded in a gradient gel and run for 90 minutes at 100V. Transfer of proteins to the nitrocellulose membrane was carried out at 60V for 20 minutes at 4 °C in order to retain low molecular weight caspases. After total protein levels were detected and imaged using the LiCor REVERT total protein stain and Odyssey CLx imaging system (Li-Cor), blots were incubated in blocking solution (5% BSA in TBS with 0.1% Tween20) for one hour, and then in rabbit anti-Drosophila DrICE$^{CST-13085S}$ (1:1000) overnight at 4°C. Fluorescent Li-Cor goat anti-Rabbit IRDye CW800 secondary antibody was then used to detect the resulting bands, and the mean signal for the 47kd band of each genotype was then normalized to the corresponding lane's total protein signal.

REAGENT or RESOURCE	SOURCE	IDENTIFIER
Antibodies		
Guinea pig anti-uninflatable (1:800)	Rob Ward	
α-DrICE^{CST9478} Rabbit anti-cleaved Drosophila ICE Asp230 (1:100)	Cell Signaling Technology (CST)	9478S
α-DrICE^{CST13085S} Rabbit anti- Drosophila ICE (1:100)	Cell Signaling Technology (CST)	13085S
Rabbit anti-PKC gamma (1:100)		
Rabbit anti-phosphorylated Src kinase (1:100)		

Mouse anti-Crumbs extracellular domain (1:25)	Developmental Studies Hybridoma Bank (DSHB) at the University of Iowa	
Mouse anti-2A12 (1:1)		
Rabbit anti-Serp (1:400)		
IRDye 800CW goat anti-Rabbit 0.5mg	Li-Cor	926-32211
Guinea-pig anti-DrICE (SK31)	Pascal Meier	SK31
Rat anti-Clathrin (Chc) (1:40)	Matthias Behr	n/a
Mouse anti-Rab5 (1:100)	BD Biosciences	610281
Mouse anti-Rab7 (1:50)	Developmental Studies Hybridoma Bank (DSHB) at the University of Iowa	Rab7
Mouse anti-Rab11 (1:100)	Fisher Scientific	BDB610656
Guinea pig anti-Melanotransferrin	Christos Samakovilis	n/a
Rabbit anti-Kune-Kune	(Nelson et al., 2010)	
Rabbit anti-Dlg		
Goat anti-mouse IgG (H+L) highly cross-adsorbed secondary antibody Alexa Fluor 488	Life Technologies	A11001
Goat anti-mouse IgM (H+L) highly cross-adsorbed secondary antibody Alexa Fluor 488	Life Technologies	A10680
Goat anti-rabbit IgG (H+L) highly cross-adsorbed secondary antibody Alexa Fluor Plus 647	Life Technologies	A32733
Goat anti-guinea pig IgG (H+L) highly cross-adsorbed secondary antibody Alexa Fluor 568	Life Technologies	A11075
IRDye 800CW Goat anti-Rabbit 0.5 mg	Li-Cor	926-32211
Critical Commercial Assays		
REVERT Total protein stain kit		
Pre-cast gel 4-15%, 15 well		
Software and Algorithms		
Fiji (ImageJ)		
Volocity Demo 5.5.1		
Leica Application Suite X (LAS X) HyVolution and colocalization calculation		
Li-Cor Image Studio Software		

References for the Methods

Brand, A.H., and Perrimon, N. (1993). Targeted gene expression as a means of altering cell fates and generating dominant phenotypes. Development *118*, 401-415.

Hay, B.A., Wassarman, D.A., and Rubin, G.M. (1995). Drosophila homologs of baculovirus inhibitor of apoptosis proteins function to block cell death. Cell *83*, 1253-1262.

Laprise, P., Beronja, S., Silva-Gagliardi, N.F., Pellikka, M., Jensen, A.M., McGlade, C.J., and Tepass, U. (2006). The FERM protein Yurt is a negative regulatory component of the Crumbs complex that controls epithelial polarity and apical membrane size. Developmental cell *11*, 363-374.

Muro, I., Berry, D.L., Huh, J.R., Chen, C.H., Huang, H., Yoo, S.J., Guo, M., Baehrecke, E.H., and Hay, B.A. (2006). The Drosophila caspase Ice is important for many apoptotic cell deaths and for spermatid individualization, a nonapoptotic process. Development *133*, 3305-3315.

Nelson, K.S., Furuse, M., and Beitel, G.J. (2010). The Drosophila Claudin Kune-kune is required for septate junction organization and tracheal tube size control. Genetics *185*, 831-839.

Robbins, R.M., Gbur, S.C., and Beitel, G.J. (2014). Non-canonical roles for Yorkie and Drosophila Inhibitor of Apoptosis 1 in epithelial tube size control. PloS one *9*, e101609.

Silva, E., Tsatskis, Y., Gardano, L., Tapon, N., and McNeill, H. (2006). The tumor-suppressor gene fat controls tissue growth upstream of expanded in the hippo signaling pathway. Current biology : CB *16*, 2081-2089.

Sweeney, N.T., Brenman, J.E., Jan, Y.N., and Gao, F.B. (2006). The coiled-coil protein shrub controls neuronal morphogenesis in Drosophila. Current biology : CB *16*, 1006-1011.

Xu, D., Wang, Y., Willecke, R., Chen, Z., Ding, T., and Bergmann, A. (2006). The effector caspases drICE and dcp-1 have partially overlapping functions in the apoptotic pathway in Drosophila. Cell death and differentiation *13*, 1697-1706.